PHYSICAL REVIEW A VOLUME 23, NUMBER 1 JANUARY 1981

Quasifree-electron bremsstrahlung induced by the projectile field

A. Yamadera, K. Ishii, and K. Sera
Cyclotron and Radioisotope Center, Tohoku University, 980 Sendai, Japan

M. Sebata and S. Morita
Department of Physics, Faculty of Science, Tohoku University, 980 Sendai, Japan

(Received 16 June 1980)

Continuum x rays from targets of Be, C, and Al bombarded with 6–40-MeV protons were observed with a Si (Li) detector. In addition to the secondary-electron bremsstrahlung (SEB), the spectra show another component, of which the high-energy limit is given by the relative kinetic energy between the projectile and orbital electrons of the target atom and by the Doppler effect. The component can well be explained in terms of the bremsstrahlung produced by the quasifree scattering of orbital electrons in the field of the projectile. The effect of the binding energy of the orbital electrons on this bremsstrahlung spectrum has been studied. From the comparison of the experimental results with theoretical predictions based on the plane-wave Born approximation and the binary-encounter approximation, the importance of the effect of secondary-electron escape from the target material on the SEB at high-projectile energies was pointed out.

I. INTRODUCTION

Continuum x-ray emission from solid or gas targets bombarded by heavy-charged particles or heavy ions has been studied by several groups of researchers.[1–9] Regarding the origin of these x rays, the following processes have been considered: Secondary-electron bremsstrahlung (SEB),[2,5–8] molecular-orbital rays (MO), radiative ionizations (RI),[3,9] radiative electron capture (REC),[1,4] nuclear bremsstrahlung,[5] and γ rays from nuclear reactions. In a case of low-energy heavy-charged-particle bombardments, SEB is generally the most predominant one among these processes. However, if the velocity of the projectile v_p is large enough in comparison with the velocity of the orbital electron, the orbital electron can be considered as free and at rest. In the center-of-mass frame, the electron collides with the projectile with the relative kinetic energy $T_r = \frac{1}{2} m_e v_p^2$ (m_e is the electron mass), and bremsstrahlung is produced by the interaction between the projectile and the orbital electron. We call radiation from this process quasifree-electron bremsstrahlung (QFEB). The spectrum of QFEB is therefore characterized by the relative kinetic energy T_r. These x rays were first observed by Schnopper *et al.*[1] in heavy-ion collisions and were called primary bremsstrahlung.[2] Theoretical calculations of this process have been performed by Jakubassa and Kleber,[3] and they called this process radiative ionizations. Experiments on QFEB have mostly been done in heavy-ion collisions, where MO x rays and REC are dominant, and QFEB by itself has not been identified.

Here, we have systematically measured the continuum x rays from Be, C, and Al targets bombarded with 6–40-MeV protons, and the results are discussed in connection with calculations of QFEB based on the plane-wave Born approximation PWBA and of SEB based on the binary-encounter approximation BEA.

EXPERIMENTAL

The general experimental setup is described elsewhere.[10] Self-supporting targets of Be, C, and Al were bombarded with protons of 6 (7 for Be target), 12, 20, 30, and 40 MeV from the AVF cyclotron of Tohoku University. Thicknesses of the targets were measured from the Rutherford scattering of 1.5-MeV protons with a Van de Graaff generator and found to be 46 mg/cm^2, about 100 μg/cm^2, and 41.8 μg/cm^2, respectively, for the Be, C, and Al targets. The continuum x-ray spectra were measured with an ORTEC Si (Li) detector of energy resolution of 160 eV for 6.4-keV x rays in the direction 135° to the proton beam. In order to avoid pileup, counting rates had been kept below about 200 cps. One of the spectra obtained is shown in Fig. 1 for the Be target bombarded with 20-MeV protons. Production cross sections for these x rays, shown in Figs. 2, 3, and 4, were obtained by correcting the spectra—best-fit curves to the experimental points—for the detection efficiency, absorption in the air path and the Mylar window of the chamber, and self-absorption in the target material. The absolute detection efficiency was determined with intensity-calibrated ^{57}Fe and ^{241}Am x-ray sources. Uncertainties in the cross sections were estimated to be about 13% for Be and Al, and about 20% for C from the following errors: background substraction 3%; target thickness 8% for Be and Al and 17% for C, count-

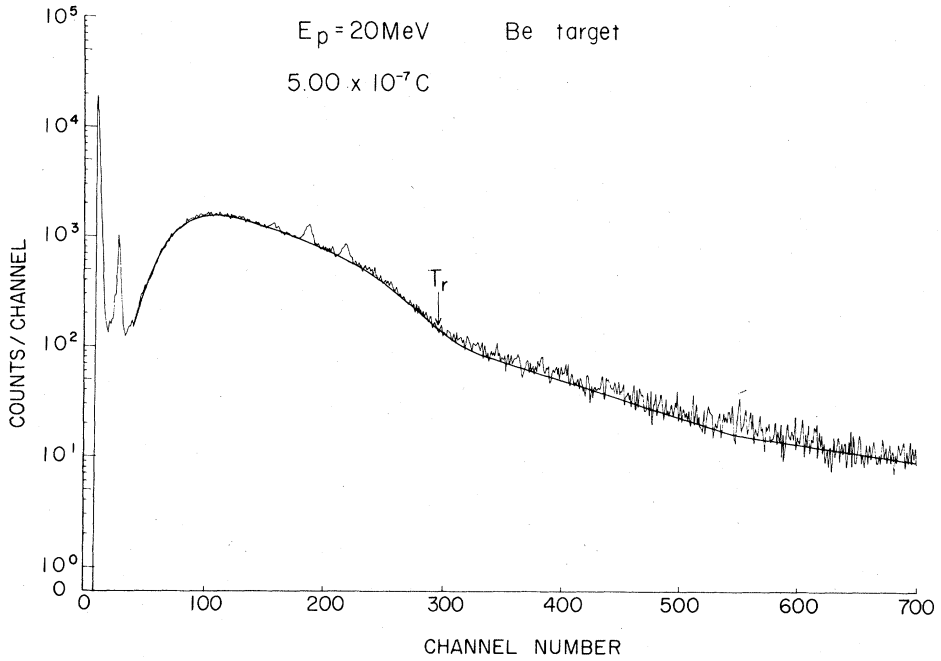

FIG. 1. A typical continuum x-ray spectrum for the Be target bombarded with 20-Mev protons.

ing statistics 2%; the detector efficiency and absorption correction, 10%.

III. THEORIES

A. Quasifree-electron bremsstrahlung (QFEB)

The production cross section of the QFEB on the basis of PWBA is expressed by[11]

$$\frac{d\sigma^{\mathrm{QFEB}}}{d\Omega d(\hbar\omega)} = \frac{N_T}{\pi} Z_p^2 \left(\frac{e^2}{\hbar c}\right)^5 a_0^2 \frac{m_e c^2}{T_r \hbar\omega} \times \left[\sin^2\theta + \tfrac{1}{4}(1+p^2)(3\cos^2\theta - 1)\ln\left(\frac{1+p}{1-p}\right) - \tfrac{1}{2}p(3\cos^2\theta - 1)\right], \quad (1)$$

where $p^2 = 1 - \hbar\omega/T_r$, N_T is the number of electrons of the target atom, Z_p is the atomic number of the projectile, a_0 is the Bohr radius, $\hbar\omega$ is the energy of the emitted photon, and θ is the angle between the directions of the projectile and the photon.

The formula of QFEB for the case where the velocity of an orbital electron is not negilible in comparison with the projectile velocity has been given by Jakubassa and Kleber[3] on the basis of PWBA. In conformity with their calculation, which takes into account the velocity distribution of the orbital electrons, the angular distribution and the spectrum of the emitted photons are expressed by

$$\frac{d\sigma^{\mathrm{QFEB}}}{d\Omega d(\hbar\omega)} = \sum_i N_i \frac{2}{\pi} Z_p^2 \left(\frac{e^2}{\hbar c}\right)^5 a_0^2 \frac{m_e c^2}{T_r \hbar\omega} \int_0^\infty dk_f \int_0^\infty dT\, \rho_i(k_z^2 + T)\, G(k_f, T, \theta), \quad (2)$$

where

$$G(k_f, T, \theta) = \left(\tfrac{1}{2}\sin^2\theta' + \cos^2\theta'\right)\frac{k_f^4}{B^2 - 4C^2} + \left(\tfrac{1}{2}\sin^2\theta' - \cos^2\theta'\right)\frac{k_f^4}{4C^2}\left(1 + \frac{B^2}{B^2-4C^2} + \frac{B}{C}\ln\left|\frac{C-k_f^2}{C+k_f^2}\right|\right) - 2\sin^2\theta' D k_f^2 \left(\frac{B}{B^2-4C^2} + \frac{1}{4C}\ln\left|\frac{C-k_f^2}{C+k_f^2}\right|\right) + \sin^2\theta' \frac{D^2 C^2}{B^2-4C^2},$$

with

$$B = (k_0 + k_z)^2 + T + k_f^2,$$
$$C = k_f\left[(k_0 + k_z)^2 + T\right]^{1/2},$$
$$D = \hbar\omega\left(\hbar\omega + U_i + \frac{\hbar^2}{2m_e}(k_z^2 + T)\right),$$
$$\cos^2\theta' = \left[(k_0 + k_z)^2\cos^2\theta + \tfrac{1}{2}T\sin^2\theta\right]/\left[(k_0 + k_z)^2 + T\right],$$
$$k_z = \frac{m_e}{\hbar^2 k_0}\left(\hbar\omega + U_i + \frac{\hbar^2 k_f^2}{2m_e} - T_r\right),$$
$$k_0^2 \equiv \frac{2m_e}{\hbar^2} T_r, \quad \text{and} \quad T \equiv k_x^2 + k_y^2,$$

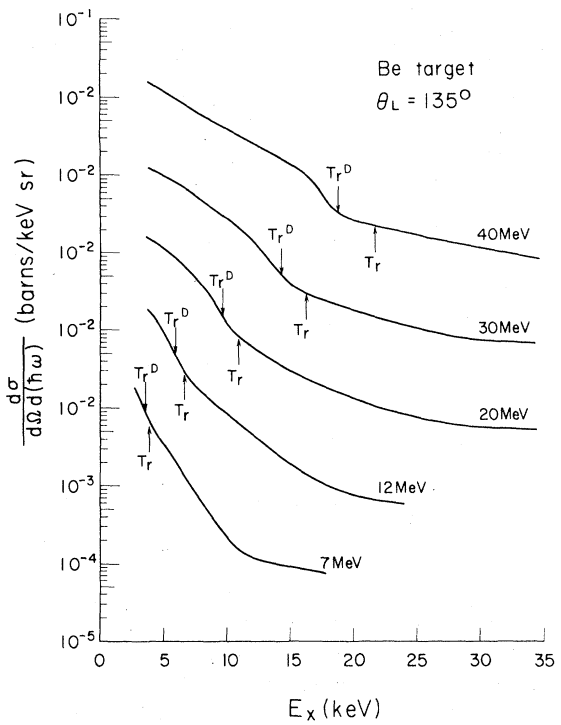

FIG. 2. Production cross section of the continuum x rays from the Be target plotted as a function of photon energy. The notation T_r is the kinetic energy of the orbital electrons in the projectile frame, and T_r^D is that in the laboratory frame taking account of the Doppler shift.

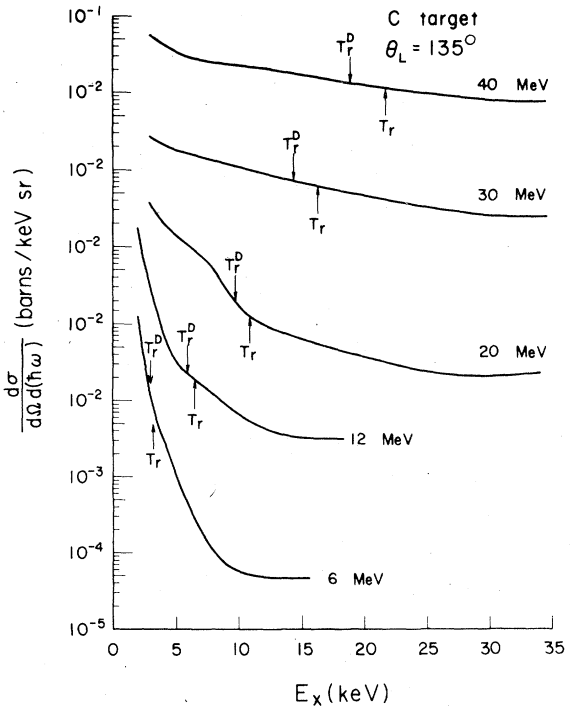

FIG. 3. Same as Fig. 2, except for the C target.

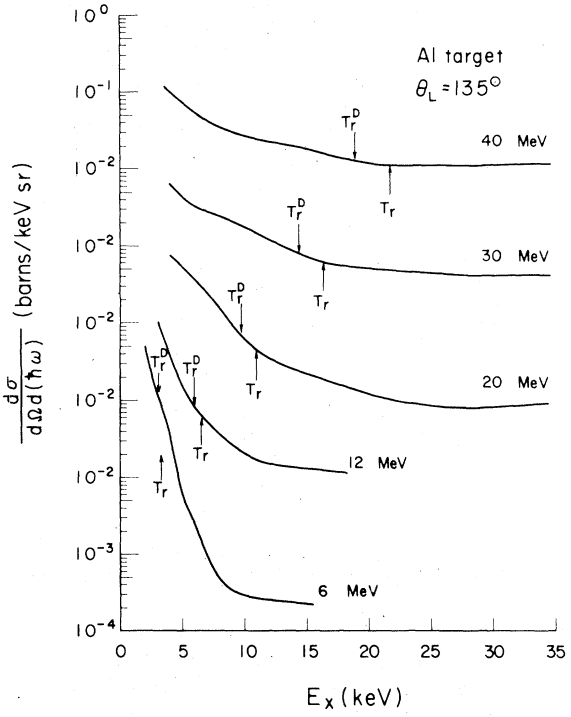

FIG. 4. Same as Fig. 2, except for the Al target.

where $\hbar k$ is the momentum of the inner-shell electron, $\hbar k_f$ is that of the ejected electron, N_i is the number of electrons in the ith shell, U_i is the ionization energy of the ith shell, $\rho_i(k^2)$ is the velocity distribution of the i-shell electron[12] and is normalized by

$$\int_0^\infty k^2\, dk\, \rho_i(k^2) = 1 . \tag{3}$$

The QFEB spectra calculated from Eq. (1) and Eq. (2) for 20-MeV proton bombardments of Be and Al targets are illustrated in Figs. 5(a) and 5(b), where it is apparent that the two calculations yield similar results for Be, but rather different results for Al. This fact reveals that the QFEB spectrum becomes increasingly dependent on the velocity distribution of the orbital electrons as the atomic number increases and the intensity decline near the high-energy limit $h\omega = T_r$ becomes less steep for higher atomic numbers.

Since the QFEB is produced in the rest frame of the projectile, a Doppler shift in the emitted-photon energy is expected; the observed x-ray energy $\hbar\omega_{ob}$ is related to the projectile-frame energy $\hbar\omega_p$ by[13]

$$\omega_{ob} = \frac{(1-\beta^2)^{1/2}}{1-\beta\cos\theta}\omega_p , \tag{4}$$

where $\beta = v_p/c$. This effect becomes large for

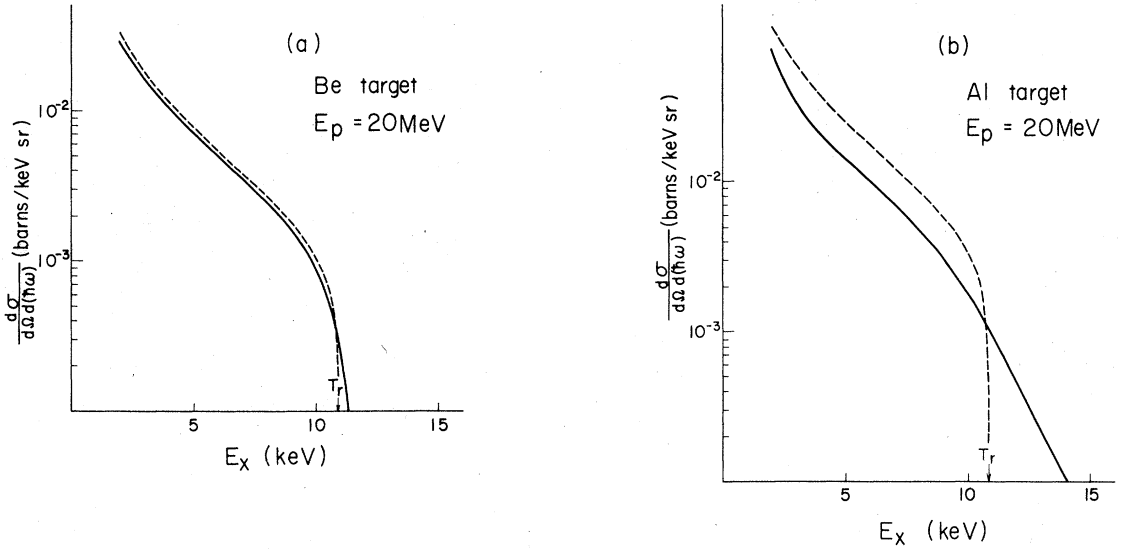

FIG. 5. Comparisons between the QFEB spectra calculated from Eqs. (1) and (2) for (a) Be and (b) Al targets.

high-energy projectiles; with 40-MeV protons, the photon energy is increased by 35% at $\theta = 0°$ and decreased by 26% at $\theta = 180°$. The cross sections for QFEB calculated from Eq. (2) and corrected for the Doppler shift are shown in Figs. 6 and 7, respectively, for the Be and Al targets, together with theoretical SEB cross sections and the experimental ones.

B. Secondary-electron bremsstrahlung (SEB)

Electrons ejected from a target atom by the projectile interact with other atoms in the target and produce bremsstrahlung. This SEB was analyzed first by Folkmann[5] and then in more detail by Ishii et al.[7,8] This continuum x-ray spectrum is characterized by the maximum energy $T_m = 2m_e v_p^2$ that can be transferred from the projectile to a free electron. In accordance with the BEA theory, the SEB cross section is given by[7]

$$\frac{d\sigma^{\mathrm{SEB}}}{d\Omega d(\hbar\omega)} = \sum_i N_i \frac{1}{2\pi} Z_p^2 \left(\frac{e^2}{\hbar c}\right)^5 a_0^2 Z_T \frac{m_e c^2}{(\hbar\omega)^2} (C_1 + C_2 \sin^2\theta), \tag{5}$$

where

$$C_1 = \int_1^\infty d\left(\frac{E_e}{\hbar\omega}\right) \int_0^\infty f_i(v_2)\, dv_2 \frac{1}{(E/\hbar\omega)^3} \frac{v_i}{v_2} \left[g_0\left(\tfrac{3}{4}f_1 - \tfrac{1}{4}f_2 + \tfrac{1}{2}f_3\right) + g_2\left(-\tfrac{1}{4}f_1 + \tfrac{3}{4}f_2 - \tfrac{3}{2}f_3\right)\right],$$

$$C_2 = \int_1^\infty d\left(\frac{E_e}{\hbar\omega}\right) \int_0^\infty f_i(v_2)\, dv_2 \frac{1}{(E/\hbar\omega)^3} \frac{v_i}{v_2} \left[g_0\left(-\tfrac{1}{8}f_1 + \tfrac{3}{8}f_2 - \tfrac{3}{4}f_3\right) + g_2\left(\tfrac{3}{8}f_1 - \tfrac{9}{8}f_2 + \tfrac{9}{4}f_3\right)\right],$$

$$f_1 = \int_1^{E_e/\hbar\omega} dt\, \frac{\ln\left(\frac{1+T}{1-T}\right)}{\ln\left(\frac{1.16}{\bar{I}}(\hbar\omega)t\right)}, \quad f_2 = \int_1^{E_e/\hbar\omega} dt\, T^2 \frac{\ln\left(\frac{1+T}{1-T}\right)}{\ln\left(\frac{1.16}{\bar{I}}(\hbar\omega)\, t\right)}, \quad f_3 = \int_1^{E_e/\hbar\omega} dt \frac{T}{\ln\left(\frac{1.16}{\bar{I}}(\hbar\omega)\, t\right)},$$

$$g_0 = \begin{cases} \dfrac{1}{6x}\left[8 + (s-x)^3\right] & \text{for } \left|\dfrac{\gamma}{4} - 1\right| < s < \infty, \\ \dfrac{s}{3x}\left[s^2 + 3x^2\right] & \text{for } 1 - \dfrac{\gamma}{4} \geq s \geq 0, \\ 0 & \text{for } s \leq \dfrac{\gamma}{4} - 1, \end{cases}$$

$$g_2 = \frac{\gamma}{2x}\left[1-\left(\frac{\gamma-2s}{2x}\right)^2\right]$$

$$+\frac{1}{7\times6\times5\times4\,x^3}\{5\times4\times3\times[(1+s)(\gamma-2s)^3-(x-1)(2x)^3]+9(\gamma+8s^2+8)\,[(1+s)(\gamma-2s)^2-(x-1)(2x)^2]$$

$$+4(8\gamma-3\gamma^2-27\gamma s^2+22s^2-24s^4-24)\,[2(x-1)(x^2+x+1)-(1+s)(2x^2+2-2s+\gamma)]\}$$

for $|\frac{\gamma}{4}| \leqslant s \leqslant \infty$.

$$g_2 = \begin{cases} \dfrac{s}{x^3}\left(\dfrac{\gamma^3}{4}+\gamma^2 s^2+\dfrac{\gamma}{3}s^2+\dfrac{4}{15}s^4+\dfrac{6}{5}\gamma s^4+\dfrac{16}{35}s^6\right) & \text{for } 1-\dfrac{\gamma}{4} \geqslant s \geqslant 0, \\ 0 \quad \text{for } s \leqslant \dfrac{\gamma}{4}-1. \end{cases}$$

Here, $E = E_e + U_i$, $x^2 = s^2 + \gamma$, $T = \sqrt{1-1/t}$, $\gamma = E/T_r$, $s = v_2/v_p$, and E_e is energy of the electron ejected from the atom, t is energy of the electron passing through the target material in units of $\hbar\omega$, Z_T is the target-atomic number, $\bar{I}$ is the average ionization potential of the target atom, and $f_i(v_2)$ is the velocity distribution of the i-shell electron[12] and is normalized as expressed by

$$\int_0^\infty f_i(v_2)\,dv_2 = 1. \tag{6}$$

The formula for SEB, expressed by Eq. (5), is more simplified than the one previously reported.[7]

As in the present case where the projectile energy is high, the energy of the secondary electrons also becomes high, and in the process of bremsstrahlung production, the relative retardation effect becomes important.[8] Further, the probability of escape of the secondary electrons from the target increases because of their high energy, and this fact reduces the yield of SEB, especially in the high-energy photon region. Calculations of SEB taking into account these effects are generally complicated because of various integral conditions. If we assume the target electron to be at rest, however, the escape effect can easily be estimated. Under this assumption, the cross section of SEB for a target of thickness D is expressed by

$$\left(\frac{d\sigma^{\mathrm{SEB}}}{d(\hbar\omega)\,d\Omega}\right)_D = \frac{1}{D}\int_0^D dx \int_{\hbar\omega}^{T_m} dE_e \int d\Omega_e \int_E^{E_e} dE_e' \left(\sigma_e(E_e,\theta_e,\psi_e)\frac{-N\,dx'}{dE_e'}\sigma^{br}(\hbar\omega, E_e', \theta')\right)$$

$$= \mathrm{const}\,\frac{1}{D}\int_0^D dx \int_{\hbar\omega}^{T_m} dE_e \int_E^{E_e} dE_e' \frac{1}{2\pi}\int d\Omega_e \frac{1}{E_e^2}\,\delta(\cos\theta_e - (E_e/T_m)^{1/2})$$

$$\times\left([\sin^2\theta' + \tfrac{1}{4}(1+t^2)(3\cos^2\theta'-1)]\log\frac{1+t}{1-t} - \frac{t}{2}(3\cos^2\theta'-1)\right)$$

$$= \mathrm{const}\,\frac{1}{D}\int_0^D dx \int_{\hbar\omega}^{T_m} dE_e \int_E^{E_e} dE_e' \frac{1}{E_e^2} f(\bar{\theta}, t), \tag{7}$$

where $t = (1-\hbar\omega/E_e')^{1/2}$, and E_e' is energy of the electron passing through the target material, (θ_e, ψ_e) is the ejection angle of the electron with respect to the incident beam, θ is the detection angle of x rays with respect to the beam, θ' is the detection angle of x rays with respect to the direction of ejection of the electron, and is related by $\cos\theta' = \cos\theta_e\cos\theta + \sin\theta_e\sin\theta\sin\theta\psi_e$, and

$$f(\bar{\theta}, t) = [\sin^2\bar{\theta} + \tfrac{1}{4}(3\cos^2\bar{\theta}-1)]\log\frac{1+t}{1-t} + \tfrac{1}{4}(3\cos^2\bar{\theta}-1)\,t^2\log\frac{1+t}{1-t} - \tfrac{1}{2}(\cos^2\bar{\theta}-1)\,t,$$

$t = (1-\hbar\omega/E_e')^{1/2}$,

$\cos^2\bar{\theta} = \cos^2\theta_e\cos^2\theta + \frac{1}{2}\sin^2\theta_e\sin^2\theta$,

since

$$\cos^2\theta_e = E_e/T_m.$$

The energy distribution $\sigma_e(E_e, \theta_e, \psi_e)$ of the ejected electrons in Eq. (7) has been given by Bonsen and Vriens[14] for electrons at rest, and the energy loss $dE_e'/-N\,dx'$ of ejected electrons in the target can be estimated from the Bethe formula,[11] in which the logarithmic term is here

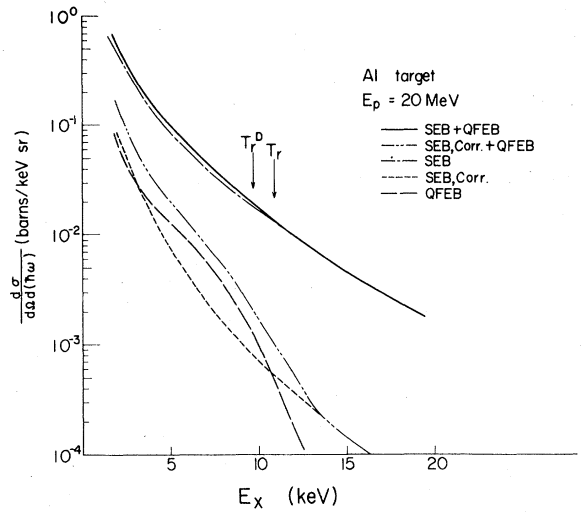

FIG. 6. Effect of electron escape from a target on the SEB spectrum is shown for the case of the Al target bombarded with 20-Mev protons.

replaced by a constant. The production cross section of the bremsstrahlung has been given by Heitler[11] on the basis of PWBA. The escape probability is taken into consideration in the lower limit E of the integration on the energy of the ejected electrons $\int dE'_e$. From the fact that an ejected electron can produce bremsstrahlung only in the target material, the lower limit E is expressed by

$$E=\begin{cases}\hbar\omega & \text{for } R(E_e)<R(\hbar\omega)+\dfrac{D-X}{\cos\theta_e},\\ R^{-1}\left(R(E_e)-\dfrac{D-X}{\cos\theta_e}\right) & \text{for } R(E_e)>R(\hbar\omega)+\dfrac{D-X}{\cos\theta_e},\end{cases} \tag{8}$$

where $R(E_e)$ is the range of an electron of energy E_e in the target material, $R^{-1}(X)$ is the electron energy corresponding to the range X, and x is the distance along the target surface between the point of beam incidence and the point where the electron is ejected. Hence, $(D-x)/\cos\theta_e$ is the path length of the ejected electron in the target on the assumption that the beam enters normal to the target surface. In the case of a target which is thick in comparison with the range of an ejected electron, Eqs. (7) and (8) give

$$\left(\frac{d\sigma^{\mathrm{SEB}}}{d(\hbar\omega)d\Omega}\right)_{D=\infty}=\text{const}\int_{\hbar\omega}^{T_m}dE_e\int_{\hbar\omega}^{E_e}dE'_e\,\frac{1}{E_e^2}f(\bar{\theta},t). \tag{9}$$

By taking the ratio of Eq. (7) to Eq. (9), we obtain the correction coefficient for the escape effect by

$$C=\left(\frac{d\sigma^{\mathrm{SEB}}}{d(\hbar\omega)\,d\Omega}\right)_D\Big/\left(\frac{d\sigma^{\mathrm{SEB}}}{d(\hbar\omega)d\Omega}\right)_{D=\infty}. \tag{10}$$

As the result, we can obtain the approximate SEB cross section taking account of the escape effect by multiplying Eq. (5) by the coefficient C.

In the present work, the thickness of the Al target was 41.8 μg/cm^2 and the escape effect cannot be neglected. The contribution of this effect to the SEB cross section is shown in Fig. 6 for 20-MeV protons. As seen in this figure, the escape effect reduces the cross section by two orders of magnitude and the relative importance of QFEB in the region of continuum x rays becomes large. It therefore becomes difficult to identify the QFEB for a thick Al target.

IV. COMPARISON BETWEEN THE THEORIES AND EXPERIMENTAL RESULTS

In the continuum x-ray spectra from a Be target shown in Fig. 2, the contribution from QFEB and its Doppler shift are clearly observable at all the proton energies, while, in the spectra for the C target shown in Fig. 3, the QFEB is identified only in the region $E_p \leq 20$ MeV. This fact is probably due to the background from Compton scattering of γ rays from the nuclear reaction $^{12}C(p,n)^{12}N$ having the threshold energy of $E_p = 18.23$ MeV. In the spectra for the Al target shown in Fig. 4, QFEB is observable, but is not so remarkable as in the case of Be and C targets. The cross sections for QFEB calculated from Eqs. (2) and (4) and for SEB calculated from Eqs. (5) and (10) are compared with the experimental results in Figs. 7 and 8, respectively, for Be and Al targets. Agreement between the theory and the experiment is quite satisfactory for the Be target. Since the Be target used is very thick (46 mg/cm^2), the escape probability of a secondary electron from the target is expected to be negligible and the SEB calculated from Eq. (5) should be a good approximation. The projectile-energy loss in the Be target amounts to about 2 and 0.6 MeV, respectively, for 9- and 40-MeV protons. On the other hand, the cross sections for QFEB and SEB, as seen in Figs. 2–4, gradually increase with an increase in the projectile energy. Hence, the theoretical calculation neglecting the effect of projectile-energy loss can well be compared with the experiment as in Fig. 7.

As seen in Fig. 4, the continuum x-ray spectra for the Al target have a plateau on the high-energy side. This plateau is thought to be due to Compton scatterings of γ rays from nuclear reactions in the Si (Li) detector. If the γ-ray energy $\hbar\omega_\gamma$ is large enough in comparison with the energy of the secondary electron E_e, the energy spectrum of secondary electrons is obtained from the cross

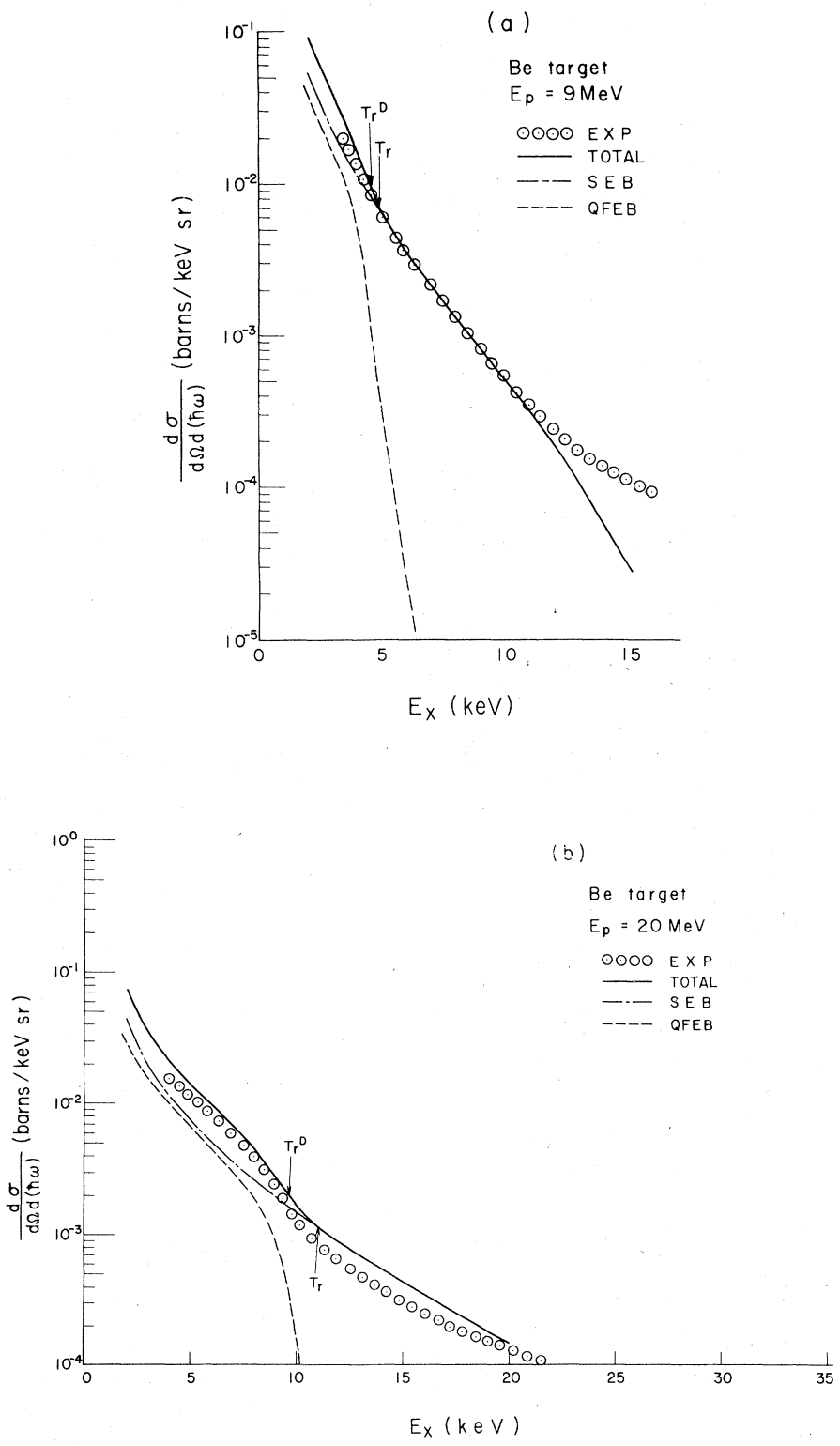

FIG. 7. Comparisons between the QFEB and SEB experimental and theoretical cross sections for the Be target.

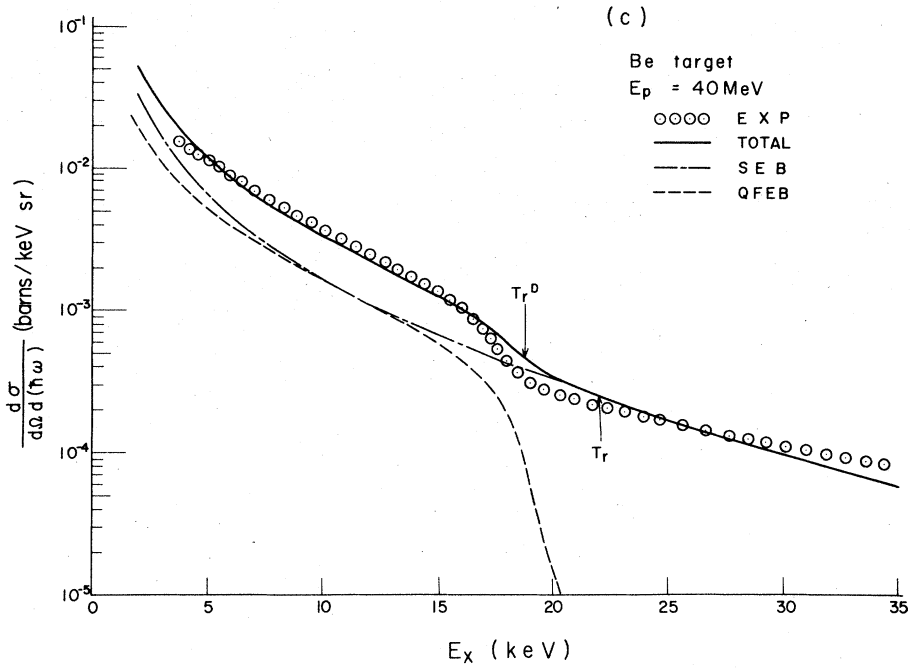

FIG. 7. (*Continued.*)

section for Compton scattering by[11]

$$\frac{d\sigma^{\text{Compt}}}{dE_e} \approx 2\pi r_0^2 \frac{m_e c^2}{(\hbar\omega_\gamma)^2}, \tag{11}$$

where r_0 is the classical electronic radius. Since the right-hand side of Eq. (11) does not contain E_e, the background spectrum due to γ rays becomes constant in the energy region from 2 keV to 35 keV. The continuous x-ray spectrum on the high-energy side in Fig. 8 is thought to be the background due to γ rays and is represented by dashed lines.

The agreement between the experiment and the calculations, shown in Fig. 8, is not good. From the comparison of the experiment with the theory in the region $\hbar\omega > T_r^D$, the correction factor for the escape effect in SEB, expressed by Eq. (10), seems to be too large. On the other hand, the experimental spectra represented in Figs. 8 (b) and 8 (c) seem to show some contribution from the QFEB, while the theoretical predictions are not so large. The situation does not change with the cross section for QFEB given by Eq. (1). As seen in Fig. 8 (c), the experimental cross sections are about one order of magnitude larger than the theoretical cross sections for QFEB. Even by taking into account the overestimation of the correction factor for the escape effect given by Eq. (10), the contribution from QFEB seen in the experimental spectra cannot be understood.

In the low-projectile energy region, the formula of QFEB, expressed by Eq. (2), does not hold. For low-energy impact, Anholt[9] has given a calculation of QFEB based on the BEA theory. His result shows that QFEB becomes effective in the region $E_p < 3$ MeV.

V. SUMMARY

Targets of Be, C, and Al foils were bombarded with proton beams of 6–40 MeV and the continuum x rays produced were measured with a Si (Li) detector. The production cross section and the spectra were analysed in terms of the quasifree-electron bremsstrahlung (SEB) processes. Calculations of QFEB and SEB have been carried out on the basis of PWBA and BEA theories, respectively. Satisfactory agreement between the calculations and the experimental results was obtained for the Be target. Large energy shifts due to the Doppler effect were observed in the spectra of QFEB and the intensity of QFEB was found to decrease with an increase in the atomic number of target. It was also found that the intensity of SEB decreases with an increase in

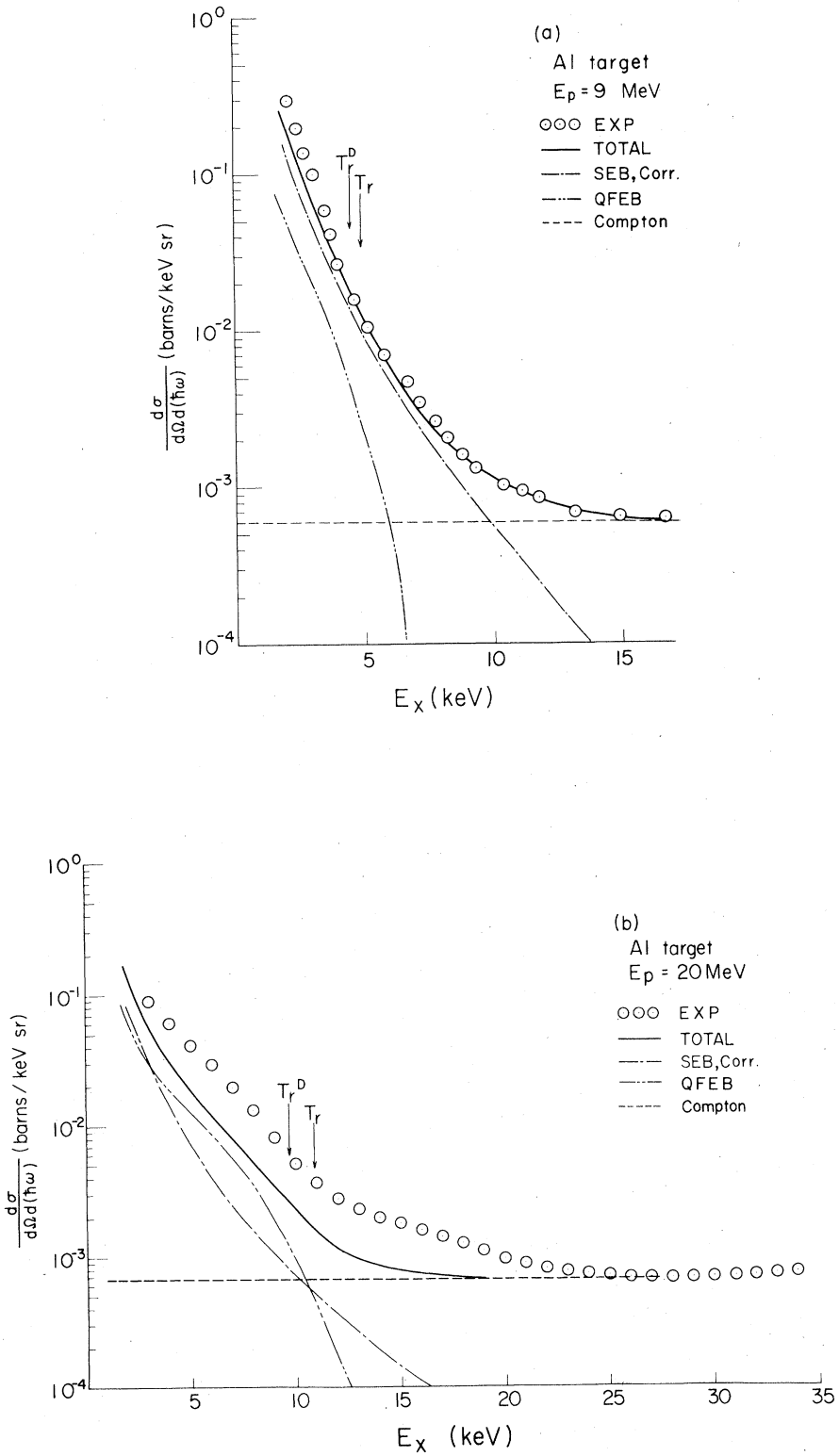

FIG. 8. Same as Fig. 6, except for the Al target.

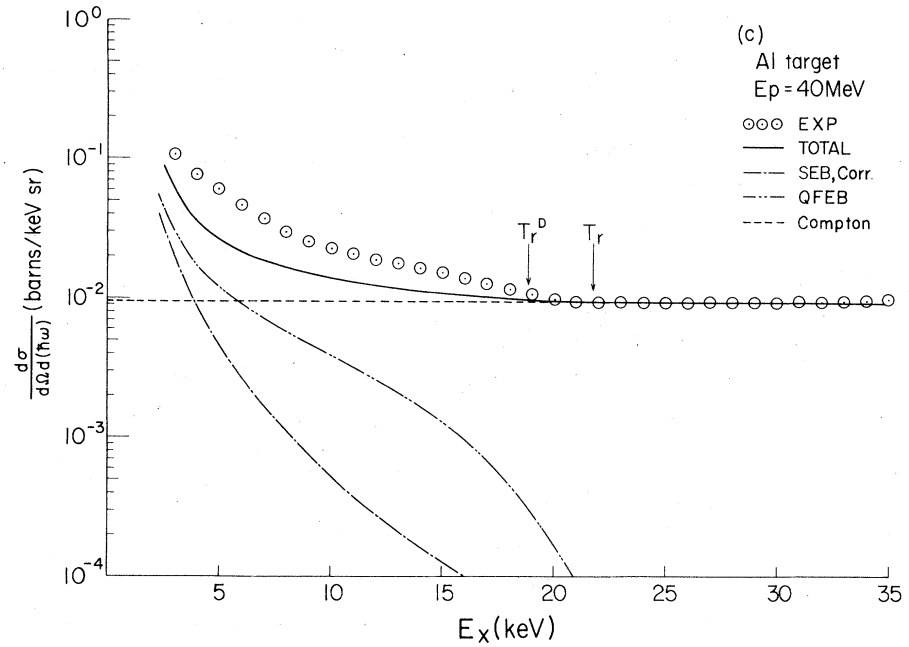

FIG. 8. (*Continued.*)

the projectile energy because of the escape of secondary electrons from the target. Even by taking into account the escape effect, good agreement between the experiment and the calculation was not obtained for the results on the Al target.

ACKNOWLEDGMENTS

The authors would like to express their appreciation to Mr. K. Hoshika, Mr. A. Ohmura, Mr. H. Ono, and Mr. S. Kan for operating the cyclotron throughout the experiment.

[1]H. W. Schnopper, J. P. Delvaille, K. Kalata, A. R. Sohval, M. Abdulwahab, K. W. Jones, and H. E. Wegner, Phys. Lett. 47A, 61 (1974).
[2]A. R. Sohval, J. P. Delvaille, K. Kalata, and H. W. Schnopper, J. Phys. B 8, L426 (1975).
[3]D. H. Jakubassa and M. Kleber, Z. Phys. A 273, 29 (1975).
[4]A. R. Sohval, J. P. Delvaille, K. Kalata, K. Kirby-Docken, and H. W. Schnopper, J. Phys. B 9, L25 (1976).
[5]F. Folkmann, C. Gaarde, T. Huus, and K. Kemp, Nucl. Instrum. Methods 116, 487 (1974).
[6]F. Folkmann, J. Borggreen, and A. Kjeldgaard, Nucl. Instrum. Methods 119, 117 (1974).
[7]K. Ishii, S. Morita, and H. Tawara, Phys. Rev. A 13, 131 (1976).
[8]K. Ishii, M. Kamiya, K. Sera, S. Morita, and H. Tawara, Phys. Rev. A 15, 2126 (1977).
[9]R. Anholt and T. K. Saylor, Phys. Lett. 56A, 455 (1976).
[10]K. Sera, K. Ishii, M. Kamiya, A. Kuwako, and S. Morita, Phys. Rev. A 21, 1412 (1980).
[11]W. Heitler, *The Quantum Theory of Radiation* (Clarendon, Oxford, England, 1954), p. 242.
[12]H. A. Bethe and E. E. Salpeter, *Quantum Mechanics of One- and Two-Electron Atoms* (Plenum, New York, 1977), p. 39.
[13]J. D. Jackson, *Classical Electrodynamics* (Wiley, New York, 1975), 2nd ed., p. 522.
[14]T. F. M. Bonsen and L. Vriens, Physica (Utrecht) 47, 307 (1970).